Title
Kinetics of the Reactions between the Criegee Intermediate CH2OO and Alcohols

Journal
The Journal of Physical Chemistry A, 122(1)

ISSN
1089-5639

Authors
Tadayon, Sara V
Foreman, Elizabeth S
Murray, Craig

Publication Date
2018-01-11

DOI
10.1021/acs.jpca.7b09773

Peer reviewed

Kinetics of the Reactions Between the Criegee Intermediate CH_2OO and Alcohols

Sara V. Tadayon, Elizabeth S. Foreman,[1] and Craig Murray[2]

Department of Chemistry, University of California, Irvine, Irvine CA 92697, USA

[1] Current address: Department of Chemistry, Massachusetts Institute of Technology, Cambridge, MA 02139, USA

[2] Email: craig.murray@uci.edu; Telephone: +1-949-824-4218

Abstract

Reactions of the simplest Criegee intermediate (CH_2OO) with a series of alcohols have been studied in a flash photolysis flow reactor. Laser photolysis of diiodomethane at 355 nm in the presence of molecular oxygen was used to produce CH_2OO and absolute number densities were determined as a function of delay time from analysis of broadband transient absorption spectra obtained using a pulsed LED. The kinetics for the reactions of CH_2OO with methanol, ethanol, and isopropanol was measured under pseudo-first order conditions at 295 K, yielding rate constants of $(1.4\pm0.4)\times10^{-13}$ $cm^3\ s^{-1}$, $(2.3\pm0.6)\times10^{-13}$ $cm^3\ s^{-1}$, and $(1.9\pm0.5)\times10^{-13}$ $cm^3\ s^{-1}$, respectively. Complementary *ab initio* calculations were performed at the CCSD(T)/aug-cc-pVTZ//CCSD/cc-pVDZ level of theory to characterize stationary points on the reaction enthalpy and free energy surfaces, and to elucidate the thermochemistry and mechanisms. The reactions proceed over free energy barriers of ~8 kcal mol^{-1} to form geminal alkoxymethyl hydroperoxides: methoxymethyl hydroperoxide (MMHP), ethoxymethyl hydroperoxide (EMHP), and isopropoxymethyl hydroperoxide (PMHP). The experimental and theoretical results are compared to reactions of CH_2OO with other hydroxylic compounds, such as water and carboxylic acids, and trends in reactivity are discussed.

Introduction

Ozonolysis of unsaturated hydrocarbons is an important oxidation process in the troposphere,[1,2] with the reaction proceeding initially via the mechanism established following decades of work in condensed phases.[3] Ozone first adds across the olefinic bond to form a cyclic primary ozonide that promptly decomposes to form a carbonyl and a carbonyl oxide, or Criegee intermediate (R_1R_2COO). In the gas phase, the energized Criegee intermediate either decomposes or is collisionally stabilized, subsequently reacting with trace atmospheric gases. Despite extensive research activity, Criegee intermediates evaded direct detection in the gas phase until relatively recently,[4,5] when photoionization mass spectrometry using tunable VUV was shown to allow specific detection of formaldehyde oxide (CH_2OO), the simplest Criegee intermediate, over its more stable isomers dioxirane and formic acid. Equally important for direct studies was the discovery that the fast reaction of photolytically-produced iodoalkyl radicals with molecular oxygen provided a convenient, high yield route to stabilized Criegee intermediate production.[5,6] Photolysis of geminal diiodoalkane precursors in the presence of molecular oxygen has been shown to be a generally viable route for production of various alkyl-substituted Criegee intermediates.[7–9]

Subsequently, there has been a proliferation of work characterizing the spectroscopy of several simple Criegee intermediates, as well as direct measurements of the kinetics of their reactions with trace atmospheric gases.[10–12] The major atmospheric sink for CH_2OO is reaction with water vapor, which is ubiquitous throughout the troposphere. While reaction with water monomer is slow, having rate constants in the range 10^{-15} to 10^{-16} cm^3 s^{-1},[5,13–15] water dimer reacts significantly faster with reported rate constants spanning $4.0–7.4\times10^{-12}$ cm^3 s^{-1} and is present at concentrations greater than many other trace gases.[14,16,17] We will use "water vapor" to refer collectively to both monomer and dimer. For larger Criegee intermediates, reactivity and unimolecular dissociation rates vary dramatically with molecular structure. Acetaldehyde oxide (CH_3CHOO) exists as *syn* and *anti*

conformers, and the reactions of *anti*-CH_3CHOO with water vapor are an order of magnitude or more faster than those of either the *syn*-CH_3CHOO or CH_2OO.[7,18,19] Acetone oxide [$(CH_3)_2COO$], on the other hand, is relatively unreactive to water vapor but undergoes rapid reaction with SO_2, suggesting that this reaction may be competitive, even in humid conditions.[8,20] Reactions of Criegee intermediates with SO_2 can contribute to sulfate aerosol particle formation and have been studied extensively.[5,7,8,15,18,21] Thermal unimolecular decomposition is also an important sink at higher temperatures, particularly for Criegee intermediates that can access the vinoxy + OH pathway, such as *syn*-CH_3CHOO and $(CH_3)_2COO$.[20,22] Reactions with trace gases that are sufficiently fast may be locally competitive with water vapor and thermal decomposition under specific conditions. Reactions with organic and inorganic acids fall into this category, with rate constants exceeding 10^{-10} cm^3 s^{-1},[23–25] and could be significant at lower temperatures and relative humidity, particularly in polluted urban environments.

While rate constants for reactions with carboxylic acids have been directly quantified relatively recently,[24,25] they have long been known as efficient gas-phase scavengers of CH_2OO from gas-phase ethene ozonolysis experiments.[26–28] Neeb *et al*. detected substituted hydroperoxide products following ethene ozonolysis in the presence of HCOOH, CH_3COOH or CH_3OH using FTIR. The products, thought to result from breaking the O–H bond of the added scavenger, were hydroperoxymethyl formate, hydroperoxymethyl acetate, and methoxymethyl hydroperoxide, respectively. From analysis of product yields, they ranked the reactivity of CH_2OO with hydroxylic compounds $H_2O \ll CH_3OH \ll HCOOH \approx CH_3COOH$.[28] Hydroperoxide products were also detected by Wolff *et al*. using HPLC/HPIC during ethene ozonolysis in the presence of HCOOH, CH_3OH, C_2H_5OH, H_2O_2, and H_2O. The expected substituted hydroperoxides were produced with particularly high yields upon addition of CH_3OH (methoxymethyl hydroperoxide, 46% yield) and CH_3CH_2OH (ethoxymethyl hydroperoxide, 38% yield). The ethene ozonolysis results suggest that rate constants for the reactions of alcohols with CH_2OO should lie between those for water and carboxylic acids.

Numerous theoretical studies have characterized Criegee intermediate reactions; Vereecken and Francisco's extensive review of theoretical studies of tropospheric reactions summarizes the period up until 2012.[29] Here we focus on theoretical studies of reactions between CH_2OO and hydroxyl compounds. The reactions of Criegee intermediates with water have been studied extensively computationally,[30–38] with most groups using model chemistries that involve geometries and harmonic frequencies calculated using varieties of density functional theory and subsequent refinement of electronic energies using CCSD(T). Mechanistically, the $CH_2OO + H_2O$ reaction proceeds via an entrance channel complex, followed by addition to form the stable adduct hydroxymethyl hydroperoxide (HMHP). The transition state is calculated to be higher in energy than the reactants, presenting a small barrier to reaction. The presence of a second water molecule suppresses the energy of the transition state, leading to a submerged barrier, and consequently larger rate constants. The transition state for the $CH_2OO + (H_2O)_2$ reaction involves a double H-atom transfer, but can also be viewed overall as an addition reaction that leads to the HMHP–H_2O complex. Transition state theory calculations predict rate constants at 298 K in the range 10^{-18}–10^{-15} $cm^3\ s^{-1}$ for the $CH_2OO + H_2O$ reaction[32–35,38] and 10^{-12}–10^{-10} $cm^3\ s^{-1}$ for the $CH_2OO + (H_2O)_2$ reaction,[32,34,35] in relatively good agreement with experimental measurements. Fewer theoretical studies have investigated the reactions of Criegee intermediates with acids,[23,30,39–41] for which the primary addition products are also substituted hydroperoxides. Entrance channel complexes and transition states are significantly more stable for the inorganic acids HCl and HNO_3, and the submerged barriers are only a few kcal mol^{-1}.[23,40,41] For carboxylic acids, the reactions with CH_2OO can proceed without a barrier to form hydroperoxymethyl esters.[39,41] Consequently, reactions with acids are significantly faster, with calculated rate constants of order 10^{-10} $cm^3\ s^{-1}$. Vereecken classifies the mechanisms as 1,2-insertion (e.g. water) or 1,4-insertion reactions (e.g. formic acid),[41] and the insertion designation has been used by others previously.[11,12] However, these reactions are entirely consistent with the IUPAC definition of addition reactions,[42] and we prefer the terms 1,2-addition and 1,4-addition,

reserving insertion to describe reactions involving atomic species that insert into chemical bonds e.g. $O(^1D) + CH_4$. To the best of our knowledge, there have been no previous theoretical studies of Criegee intermediate reactions with alcohols.

The kinetics of the reactions of Criegee intermediates with the alcohols methanol, ethanol and isopropanol is the subject of this work. Alcohols are found throughout the troposphere and have primarily biogenic sources. After methane, methanol is the most abundant organic compound in the atmosphere and is primarily released during plant growth, although other sources include plant decay, biomass burning, and industrial and vehicular emissions.[43] Average methanol mixing ratios range from 1 ppbv over the remote ocean to 20 ppbv for urban areas and forests.[44] Ethanol is produced from vegetation and plant litter, with smaller anthropogenic contributions from the use of commercial and industrial solvents, resulting in typical mixing ratios of 100 pptv in remote areas and 1–10 ppbv in urban areas.[45] In regions where a sizeable proportion of vehicles run on ethanol-blended fuels, peak mixing ratios of several hundred ppbv have been measured.[46] A study of alcohol concentrations in Osaka reported average mixing ratios of isopropanol that are close to those of methanol and ethanol.[47] Other alcohols have been identified in plant emissions,[48] though field measurements of the mixing ratios are scarce.

In this paper, we describe a combined experimental and computational study exploring the kinetics and mechanisms of the reactions between CH_2OO and a series of alcohols. Rate constants for the reactions of methanol, ethanol, and isopropanol have been measured at 295 K using broadband transient absorption spectroscopy. Complementary *ab initio* calculations have been performed to map out the reaction pathways on the enthalpy and free energy surfaces. Reactivity trends across families of hydroxylic and related compounds are shown to correlate well with the reactant gas-phase acidities, moderated by the mechanism of the reactions. Possible atmospheric implications

and the fates of the substituted hydroperoxide products of reactions between Criegee intermediates and alcohols are discussed.

Experimental and computational methods

Flash kinetics measurements were performed in a flow reactor using single-pass broadband transient absorption spectroscopy, the details of which have been described previously, with some minor modifications.[23,49] All measurements were performed at 295 K and a total pressure of 80–100 Torr. Briefly, CH_2OO formation is initiated by pulsed laser photolysis of CH_2I_2 (Alfa Aesar, 99%) at 355 nm (Continuum Surelite III-10 or Quantel Brilliant B, typical pulse energies 10–14 mJ cm^{-2}) in the presence of a large excess O_2. Photolytically generated CH_2I radicals react rapidly with O_2 to form CH_2OO with high yield.[50–53] Transient absorption spectra were recorded in the wavelength range 360–390 nm as a function of time after photolysis by dispersing the transmitted output of a pulsed broadband UV LED (LightSpeed Technologies, HPLS-36, 500 ns duration) in a spectrograph (Andor SR303i with iDus 420). The UV LED was nominally centered at 365 nm and had an approximately Gaussian output with FWHM of ~10 nm. Absorption spectra were collected at a repetition rate of 10 Hz and 300 individual spectra were averaged for each photolysis-probe time delay.

For the present experiments, the length of the stainless-steel flow reactor was increased from 50 cm to 160 cm (total volume ~1.5 L), improving the sensitivity, and choked flow orifices of various diameters (O'Keefe) were used to regulate the gas flows rather than mass flow controllers. The orifices were calibrated using a mass flow controller (Alicat) to accurately determine the mass flows under the experimental backing pressure conditions. The total gas flow to the cell was ~3 sLpm, with individual flows set to yield fractional concentrations of ~0.1% CH_2I_2, ~10% O_2, and N_2 balance. For the kinetics measurements, the alcohols CH_3OH (Fisher Scientific, 99.8%), CH_3CH_2OH (Sigma Aldrich, 99.5%), and $(CH_3)_2CHOH$ (Fisher Scientific, 99.9%) were introduced by flowing N_2 through a bubbler containing the liquid sample. The bubbler was immersed in a temperature-controlled water bath to

stabilize the vapor pressure of the alcohol. For the kinetics measurements, fractional alcohol concentrations were varied over the range 0.3%–4.0% (absolute concentrations of 10^{16} to 10^{17} cm^{-3}) by using choked flow orifices with different diameters. Alcohol concentrations were three to four orders of magnitude greater than typical peak concentrations of CH_2OO ($\sim 10^{13}$ cm^{-3}), ensuring pseudo-first order conditions. Alcohol concentrations in the flow reactor (in cm^{-3}) were estimated using

$$[\mathrm{ROH}] = \chi F P_{\mathrm{tot}} \frac{N_{\mathrm{A}}}{10^3 RT} \qquad \text{(E1)}$$

where χ is the mole fraction of the alcohol in the ROH/N_2 gas flow, F is the fraction of that flow relative to the total gas flow, P_{tot} is the total pressure (in atm) maintained in the flow reactor during the measurements, and R is the gas constant in L atm mol^{-1} K^{-1}. The vapor pressures (and corresponding mole fractions) for methanol, ethanol, and isopropanol were 108 Torr (χ = 0.092), 49 Torr (χ = 0.044), and 36 Torr (χ = 0.033), respectively, at the water bath temperature of 295 K. The smaller values of χ for ethanol and isopropanol necessitated increased ROH/N_2 gas flows to achieve a range of concentrations like that of methanol. An independent flow of N_2 controlled by a mass flow controller was used to balance changes in F and maintain a constant total pressure. Potential sources of error in using Equation E1 to determine alcohol concentration are evaporative cooling of the liquid and lack of vapor/liquid equilibration in the N_2 flow, both of which could potentially lead to systematic overestimation of the alcohol concentration, especially at higher flow rates. Instability and non-linearity in the CH_2OO loss rate with flow rate were observed only in the absence of temperature stabilization.

Complementary *ab initio* calculations were performed to characterize stationary points on the potential energy surfaces for the reactions of CH_2OO with methanol, ethanol, and isopropanol. Optimized geometries and harmonic frequencies for reactants, entrance channel complexes,

transition states, and products were calculated at the CCSD/cc-pVDZ level of theory and the electronic energies were subsequently refined using single point CCSD(T)/aug-cc-pVTZ calculations. Intrinsic reaction coordinate (IRC) calculations were used to confirm correspondence of the transition states with the correct reactant and product species. The *ab initio* calculations are not exhaustive, and the reported structures represent only the lowest energy conformations identified. Thermodynamic functions at 298.15 K were evaluated within the rigid-rotor harmonic oscillator (RRHO) approximation and may be subject to some degree of error due to the presence of low frequency modes or internal rotors. All calculations were performed using the MOLPRO 2012.1 program.[54]

Results

Broadband transient absorption spectroscopy following laser flash photolysis was used to directly measure rate constants for the reactions of CH_2OO with methanol, ethanol, and isopropanol:

$$CH_2OO + CH_3OH \rightarrow \text{products} \quad \text{(R1)}$$

$$CH_2OO + CH_3CH_2OH \rightarrow \text{products} \quad \text{(R2)}$$

$$CH_2OO + (CH_3)_2CHOH \rightarrow \text{products} \quad \text{(R3)}$$

All experiments were performed at a temperature of 295 K and at total pressures of 80–100 Torr. Photolysis of CH_2I_2 at 355 nm was used to generate CH_2I radicals, which react rapidly (k_4 = 1.37–1.82×10^{-12} cm^3 s^{-1}) with O_2, to yield CH_2OO and other products:[6,55,56]

$$CH_2I + O_2 \rightarrow CH_2OO + I \quad \text{(R4a)}$$

$$CH_2I + O_2 \rightarrow HCHO + IO \quad \text{(R4b)}$$

$$CH_2I + O_2 + M \rightarrow CH_2IOO + M \quad \text{(R4c)}$$

Branching between reactions R4a–c is pressure-dependent and, across the 80–100 Torr range used in the current experiments, the fractional yield of CH_2OO is estimated to be ~0.67.[52,53]

1. Transient absorption spectroscopy

Single-pass transient absorption spectra of the $\tilde{B}^1A'$–$\tilde{X}^1A'$ transition of CH_2OO were recorded over the wavelength range 360–390 nm, using a UV LED with an approximately Gaussian spectral profile (centered at 365 nm, FWHM 10 nm), capturing several characteristic vibronic features on the red edge of the absorption band.[49,56,57] IO, an unavoidable by-product of the $CH_2I + O_2$ reaction, also absorbs in the probe spectral window.[58] A small fraction of the total IO is produced directly via Reaction R4b but it is formed predominantly by secondary chemistry, resulting in very different kinetics.[52,55,59–61] The upper panel of Figure 1 shows transient absorption spectra recorded at selected time delays after the photolysis laser pulse in the absence of alcohol and in the presence of 9.7×10^{16} cm^{-3} of methanol . The absorbance reaches a maximum rapidly (Δt < 10 μs) and clearly shows the diffuse vibrational structure that is characteristic of CH_2OO. The overall absorbance decreases at longer delays, and the vibrational structure becomes increasingly indistinct; at the longest delay times, the spectrum is dominated by the IO continuum absorption. The addition of alcohol has little effect on the spectra acquired at either short or long delays, but increases the rate at which CH_2OO is lost.

Absolute concentrations of CH_2OO and IO were obtained by fitting the transient spectra at each time delay to a linear combination of the wavelength-dependent absorption cross sections of CH_2OO and IO,[49,58]

$$A(\lambda)/l = [\mathrm{CH_2OO}]\sigma_{\mathrm{CH_2OO}}(\lambda) + [\mathrm{IO}]\sigma_{\mathrm{IO}}(\lambda) \quad \text{(E2)}$$

The absorbance at early times is almost exclusively due to CH_2OO, which is both formed and removed much faster than IO. The maximum CH_2OO concentration of $\sim2.5\times10^{13}$ cm^{-3} is reached

approximately 10 μs after photolysis. The peak [CH_2OO] is consistent with the initial [CH_2I_2] of 4×10^{15} cm^{-3}, measured directly using absorption spectroscopy, and a fractional dissociation of <1%,[23] estimated using the photolysis laser fluence and the CH_2I_2 absorption cross section at 355 nm.[62,63] The residence time of the gas in the cell is ~4 s and while the effect of varying the repetition rate was not directly examined, the measured absorbance was observed to return to background within the 100 ms period between photolysis pulses and the peak concentrations of CH_2OO were consistent over extended time periods.

In the absence of additional reactants, [CH_2OO] decayed over several hundred microseconds, and was completely removed by 400 μs. Over the range of concentrations used, the addition of alcohol left the rise time and peak concentrations of CH_2OO unaffected but increased the overall loss rate. The lower panel of Figure 1 shows typical [CH_2OO] time profiles in the absence and presence of methanol in the flow reactor. Several processes contribute to CH_2OO loss, even in the absence of alcohol. On the sub-millisecond time scale of the measurements, diffusion followed by wall loss is negligible and thermal unimolecular decomposition, for which rates of 0.2–11.6 s^{-1} have been reported,[13,21,64,65] is also much too slow to contribute significantly. The major loss processes are gas-phase reactions with other species that are present in the flow reactor, in particular I atoms and residual CH_2I_2 precursor, as well as the self-reaction. The kinetic model used to describe the time dependence of [CH_2OO] incorporates formation and loss processes, the former depending on the reaction of the photolytically-produced CH_2I with O_2. The coupled differential rate equations for [CH_2I] and [CH_2OO] can be written as

$$\frac{d[\mathrm{CH_2I}]}{dt} = -k_4'[\mathrm{CH_2I}] \tag{E3}$$

$$\frac{d[\mathrm{CH_2OO}]}{dt} = +k_{\mathrm{form}}'[\mathrm{CH_2I}] - k_{\mathrm{loss}}'[\mathrm{CH_2OO}] - 2k_{\mathrm{self}}[\mathrm{CH_2OO}]^2 \tag{E4}$$

where primes indicate pseudo-first order rate constants. CH_2I is consumed (Equation E3) in a pseudo-first order process by reaction with excess O_2, with rate constant $k'_4 = k_4[O_2]$. Equation E4 describes the time dependence of the CH_2OO concentration. The first term describes the formation rate, where $k'_{\text{form}} = k_{4a}[O_2] = \Phi_{4a}k_4[O_2]$. The second term approximates losses due to reactions with other species as pseudo-first order processes; that is, $k'_{\text{loss}} = k'_0 + k_{\text{ROH}}[\text{ROH}]$ where $k'_0 = \sum k'_{X,i}$ and the $k'_{X,i}$ are pseudo-first order rate constants for background reactions that occur in the absence of the alcohol reactant. Finally, the third term describes loss via self-reaction. Values for k_{self} in the range 6.0–8.0×10^{-11} cm^3 s^{-1} have been reported,[21,52,66] indicating that self-reaction is fast. However, numerically modeling the $[CH_2OO]$ time dependence by neglecting pseudo-first order loss and considering only loss due to self-reaction predicts a CH_2OO lifetime of about 2 ms while the experimentally observed lifetime is <0.5 ms. While the self-reaction is fast, it is not sufficiently fast on its own to account for the observed loss of CH_2OO.

Equation E4 is a Ricatti differential equation, for which the analytical solution is too complicated to be useful as a fitting function. In our previous work on the reactions of CH_2OO with inorganic acids, we found that loss was well-described by a simple exponential decay, which suggested that self-reaction did not contribute significantly.[23] As will be demonstrated below, neglecting the self-reaction term in Equation E4 has no effect on the change in k'_{loss} measured as a function of added alcohol concentration. If self-reaction is neglected, the integrated rate equation describing the $[CH_2OO]$ time dependence becomes a simple exponential rise and fall:

$$[CH_2OO]_t = [CH_2I]_0 \frac{k'_{\text{form}}}{k'_{\text{loss}} - k'_{\text{form}}} \left(e^{-k'_{\text{form}}t} - e^{-k'_{\text{loss}}t} \right) \quad \text{(E5)}$$

Equation E5 provides an excellent fit to the experimental data, as shown in Figure 1. The rising edge is characterized by the greater of k'_{form} and k'_{loss}, and typical values of ~10^5 s^{-1} are consistent with

249 the expected rate of formation based on reported rate constants for Reaction R4, the O_2
250 concentration, and the pressure-dependent Criegee intermediate yield.

251 To explore the effect on the loss rates of neglecting the self-reaction, CH_2OO concentration time
252 profiles were simulated by solving Equation E4 numerically for a selected range of k'_{loss} values
253 spanning the approximate range determined by fitting the experimental data. The CH_2OO formation
254 and self-reaction rate constants were fixed using previously reported values.[6,21,67] Fitting the
255 simulated [CH_2OO] time profiles to Equation E5 yielded values of k'_{loss} that were systematically, but
256 uniformly, larger than the input value. The addition of alcohol increases the observed CH_2OO loss
257 rate, as determined by fitting to the exponential rise and fall. While neglecting self-reaction leads to
258 a systematic overestimate of k'_{loss}, the uniformity of the overestimate means that it has no significant
259 effect on the increase in the loss rate that occurs in the presence of the alcohol. Using k_{self} = 7×10^{-11}
260 $cm^3\ s^{-1}$,[21,52,66] we estimate that the fraction of CH_2OO lost to self-reaction is less than 0.06 in
261 background measurements, and decreases even further in the presence alcohol.

262 Figure 2 shows pseudo-first order plots of k'_{loss} as a function of [ROH] for each of the three alcohols.
263 The horizontal line represents the average background loss rate, k'_0, which incorporates any
264 systematic overestimate of k'_{loss} introduced by neglecting the CH_2OO self-reaction. For all three
265 alcohols, k'_{loss} increases linearly with alcohol concentration and the intercept agrees with k'_0 to
266 within their mutual uncertainties. The slopes of the pseudo-first order plots correspond to the
267 bimolecular rate constants k_{ROH} and are similar for all three alcohols. Reaction with ethanol is fastest,
268 with rate constant k_{EtOH} = $(2.3\pm0.6)\times10^{-13}$ $cm^3\ s^{-1}$, followed by isopropanol with k_{iPrOH}= $(1.9\pm0.5)\times10^{-13}$
269 $cm^3\ s^{-1}$, and finally methanol with k_{MeOH} = $(1.4\pm0.4)\times10^{-13}$ $cm^3\ s^{-1}$. Reported error limits are
270 propagated from the 1σ statistical uncertainties from the fits, which are weighted by the uncertainty
271 in k'_{loss}, and an estimated 25% systematic uncertainty in the alcohol concentration.

Ab initio calculations at the CCSD(T)/aug-cc-pVTZ//CCSD/ac-pVDZ level were performed to characterize minima and saddle points on the potential energy surfaces for the reactions of CH_2OO with methanol, ethanol, and isopropanol. Cartesian coordinates and images are collated in the Supplementary Information. Figure 3 shows the standard enthalpy and standard free energy profiles relative to the reactants for the CH_2OO + CH_3OH reaction, evaluated at a pressure of 1 am and a temperature of 298.15 K. Very similar enthalpy and free energy profiles are found for the ethanol and isopropanol reactions, with differences at each point typically being only a few kcal mol^{-1}. The calculated thermochemical data for all three alcohol reactions are compiled in Table 1.

The reactions proceed by first forming hydrogen-bonded complexes between the alcohol and CH_2OO ($\Delta H \approx -8$ kcal mol^{-1} relative to reactants). Modest geometrical rearrangements are required to reach the transition states from the complexes. The reactions proceed via an 1,2-addition mechanism, in which the alcohol adds across the Criegee intermediate to form geminal alkoxymethyl hydroperoxide ($ROCH_2OOH$) primary products. Overall, forming methoxymethyl hydroperoxide (MMHP), ethoxymethyl hydroperoxide (EMHP), and isopropoxymethyl hydroperoxide (PMHP), is exothermic by $\Delta H \approx -48$ kcal mol^{-1}. The addition transition states, TS_{add}, are first order saddle points on the reaction potential energy surface, characterized by imaginary frequencies in the range $360i$–$390i$ cm^{-1} and located at $\Delta H \approx +4$ kcal mol^{-1} with respect to the complexes. That is, the enthalpic barrier to reaction is submerged. For the CH_2OO + CH_3OH reaction, an alternative transition state was identified in which the alcohol undergoes 1,2-addition across CH_2OO via the C–H bond of the methyl group in the eclipsed position relative to the OH group, forming 2-hydroxyethyl hydroperoxide (2-HEHP). While the reaction forming 2-HEHP is slightly more exothermic than that leading to MMHP, the barrier of $\Delta H \approx +21$ kcal mol^{-1} is significantly higher and inaccessible at 298 K. Analogous pathways likely exist for reactions of ethanol and isopropanol, but were not pursued computationally.

Two energetically accessible decomposition pathways were identified for the alkoxymethyl hydroperoxide primary products. First, homolytic cleavage of the weak peroxide bond leads to formation of OH and an alkoxymethoxy radical ($ROCH_2O$), which lie at $\Delta H \approx -4$ kcal mol^{-1} relative to the reactants. The second decomposition pathway is the highly exothermic ($\Delta H \approx -70$ kcal mol^{-1} with respect to the hydroperoxide) elimination of water to produce the corresponding alkyl formates (ROCHO). The H_2O elimination transition states, TS_{elim}, are characterized by imaginary frequencies of approximately 1620i cm^{-1}, and involve formation of water from the peroxy OH group and an α-H atom. The enthalpic barrier to water elimination from the alkyl hydroperoxide is almost thermoneutral with respect to the reactants. The free energy surface paints a slightly different picture (see Figure 3 and Table 1). The entrance channel complexes are entropically unstable with respect to the reactants, with $\Delta G \approx +3$ kcal mol^{-1} and the free energy barriers for the initial 1,2-addition reactions are not submerged, and are found at $\Delta G \approx +8$ kcal mol^{-1}. Decomposition of the alkoxymethyl hydroperoxides via water elimination is inhibited by +10 kcal mol^{-1} barriers for TS_{elim} on the free energy surfaces, but the radical pathways remain accessible.

Discussion

The rate constants for the reactions of CH_2OO with methanol, ethanol, and isopropanol are similar, with $k_{ROH} \approx 10^{-13}$ cm^3 s^{-1} at 295 K. The alcohol reactions are significantly faster than reaction with water monomer, $k_{H_2O} \approx 10^{-15}$ cm^3 s^{-1},[5,13,15] but much slower than reactions with carboxylic acids, $k_{RCOOH} \approx 10^{-10}$ cm^3 s^{-1}.[24,25] While this article was under review, Orr-Ewing and co-workers reported direct kinetics measurements of reactions R1 and R2 using cavity ring-down spectroscopy. They found a small negative temperature dependence for the reactions, with rate constants of $k_{MeOH} = (1.1^{+1.0}_{-0.6})\times10^{-13}$ cm^3 s^{-1} and $k_{EtOH} = (1.2^{+1.9}_{-0.8})\times10^{-13}$ cm^3 s^{-1} at 295 K, in good agreement with this work.[68] The relative magnitudes of the rate constants determined from direct kinetics measurements agree with the reactivity trend inferred from ethene ozonolysis studies using hydroxylic species as Criegee

intermediate scavengers by Neeb *et al.*: $H_2O \ll CH_3OH \ll HCOOH \approx CH_3COOH$.[28] Tobias and Ziemann found the same reactivity trend for the C13 Criegee intermediate formed in the ozonolysis of 1-tetradecene and noted that the reaction rates depended primarily on the reactant functionality with little variation among different alcohols or carboxylic acids.[69] In all the reactions of CH_2OO involving hydroxylic compounds, the primary products in both the gas and liquid phases are substituted hydroperoxides.[3,27,28] Considering methanol and formic acid to be representative of alcohols and carboxylic acids, the primary products are methoxymethyl hydroperoxide (CH_3OCH_2OOH, MMHP) and hydroperoxymethyl formate ($HC(O)OCH_2OOH$, HPMF), while the reaction of CH_2OO with water forms hydroxymethyl hydroperoxide ($HOCH_2OOH$, HMHP). While these reactions all proceed via addition mechanisms to form substituted hydroperoxides, the rate constants span six orders of magnitude.

The *ab initio* calculations find a submerged barrier for the $CH_2OO + CH_3OH$ reaction of $\Delta H = -4.1$ kcal mol^{-1} at 298 K, while analogous calculations for the $CH_2OO + H_2O$ reaction locate the transition state at $\Delta H = +0.7$ kcal mol^{-1}. On the free energy surface the respective barriers are +12.2 kcal mol^{-1} and +8.3 kcal mol^{-1}. The ratio of the rate constants for the methanol and water reactions can be estimated using the Eyring equation

$$\frac{k_{CH_3OH}}{k_{H_2O}} = \exp\left(-\frac{\Delta\Delta G}{RT}\right)$$

where $\Delta\Delta G$ is the difference between the *ab initio* free energy barriers. The reaction of CH_2OO with methanol is predicted to have a rate constant 740 times larger than that of water at 298 K. Using the rate constant of $k_{MeOH} = 1.4\times10^{-13}$ cm^3 s^{-1} determined in this work, the rate constant for the $CH_2OO + H_2O$ reaction is predicted to be 1.9×10^{-16} cm^3 s^{-1}, in good agreement with experimental measurements.[5,13,14]

If complex formation is assumed to be a pre-requisite for reaction and equilibrium is established, the reactions of CH_2OO + ROH [R = H, CH_3, C_2H_5, $(CH_3)_2CH$] can modelled as two step composite reaction:

$$CH_2OO + ROH \rightleftharpoons [CH_2OO\cdots ROH] \rightarrow \text{products}$$

The overall rate constant k_{ROH} can therefore be expressed as

$$k_{ROH} = K_{eq} k_{add}$$

K_{eq} is the equilibrium constant for complex formation, which can be evaluated from the standard free energy change in going from reactants to the complex, $[CH_2OO\cdots ROH]$. The rate constant for the addition step, k_{add}, can be evaluated using canonical transition state theory (CTST)

$$k_{add} = \kappa \frac{k_B T}{h} \exp\left(-\frac{\Delta G}{RT}\right)$$

where κ is the tunneling correction factor and ΔG is the standard free energy change associated with going from the complex to the transition state. Previous calculations characterizing the $CH_2OO + H_2O$ reaction have found relatively small tunneling correction factor of κ = 1.24 by modelling potential energy as an unsymmetrical Eckart potential, and never greater than a factor of three for reactions involving a range of Criegee intermediates.[33] A crude estimate of the tunneling correction factor can be obtained using the one-dimensional Wigner approximation

$$\kappa = 1 + \frac{u^{\star 2}}{24}$$

where $u^\star = h\nu^\star / kT$ and $\nu^\star$ is the frequency of the imaginary mode. For the $CH_2OO + H_2O$ reaction, $\nu^\star$ = 475i cm^{-1}, suggesting a tunneling correction factor of 1.22. The imaginary frequencies and relative barrier heights for the 1,2-addition reactions are similar, and we estimate values for κ in the range 1.12–1.14. Uncertainties in the values of ΔG arising from use of the RRHO approximation are likely to introduce errors of a similar or larger magnitude. The predicted rate constants are in surprisingly

good agreement with the values determined experimentally. The calculated rate constant of 3.1×10^{-16} cm^3 s^{-1} for the $CH_2OO + H_2O$ reaction is in excellent agreement with the value reported by Berndt *et al*.[13] and consistent with the upper limits reported by Welz *et al*. and Chao *et al*.[5,14] The rate constants for the reaction of methanol, ethanol, and isopropanol are calculated to be 2.5×10^{-13} cm^3 s^{-1}, 4.8×10^{-13} cm^3 s^{-1}, and 6.6×10^{-13} cm^3 s^{-1}, respectively. The CTST calculations predict rate constants that are the correct order of magnitude, although the experimental trend is not reproduced. This approach cannot, however, be used to calculate a rate constant for the HCOOH reaction, which proceeds by a barrierless association to form hydroperoxymethyl formate (HPMF) without the formation of a stable reactant complex.[30,39] The rate constants predicted for the reactions of the inorganic acids HCl and HNO_3 are significantly overestimated, suggesting that the large rate constants observed for reactions of carboxylic and inorganic acids approach the collision limit and may be controlled by long-range interactions between the reactants.[23,25]

While reactions of CH_2OO with hydroxylic compounds form analogous substituted hydroperoxide products, the *ab initio* results indicate that the mechanism for the fast reactions of nitric acid and carboxylic acids with CH_2OO is different from that of the far slower reactions of water and alcohols. Figure 4 shows transition state geometries and force vectors associated with the imaginary mode for the reactions of CH_2OO with H_2O, CH_3OH, and HNO_3, calculated at the CCSD/cc-pVDZ level of theory. Water and methanol (and alcohols more generally) add across CH_2OO i.e. the hydroxyl H-atom is transferred to the terminal O-atom of the Criegee intermediate, while a new bond simultaneously forms between the hydroxyl O-atom and the Criegee C-atom. For HNO_3 (and HCOOH) however, the new C–O bond is formed not between the hydroxylic O-atom, but rather the nitrosyl (carbonyl) O-atom.[23,30,39–41] Consequently, we make a distinction between a 1,2-addition mechanism for the reactions of water and alcohols, and a 1,4-addition mechanism for the reactions of nitric acid and carboxylic acids.[41] The $CH_2OO + HCl$ reaction can also be classified as a 1,2-addition, while $CH_2OO + (H_2O)_2$ can be construed as a 1,4-addition of the water dimer across the Criegee intermediate leading

to the HMHP–H_2O complex as the adduct.[23,31–34] In general, the 1,4-addition mechanism is associated with reactions of hydroxylic compounds that have larger rate constants, viz. HNO_3, RCOOH, and $(H_2O)_2$. One possible reason for the lower energies of the 1,4-addition transition states (where they exist) is structural. The distance between the C-atom and the terminal O-atom of CH_2OO (the atoms that participate in bond-formation) is about 2.2 Å. The distance between the hydroxylic H-atom and carbonyl/nitrosyl O-atom in formic and nitric acids is 2.4 Å and 2.1 Å, respectively, while the OH bond in alcohols is < 1 Å. The O–H···O moiety in both the entrance channel complex and transition state has a bend angle of ~150° in the CH_2OO + ROH reactions and the resulting strained five-membered transition states lead to greater barrier heights. The geometric constraints are relaxed to some degree in the fast reaction of HCl with CH_2OO ($k_{HCl} = 4.6\times10^{-11}$ cm^3 s^{-1}), which also proceeds by a 1,2-addition mechanism and a five-membered transition state,[23] by the longer HCl bond length of $r_{HCl} \approx$ 1.28 Å. As a result, the free energy barrier is reduced to +0.6 kcal mol^{-1}, calculated at the same level of theory. In contrast, the species that react by the 1,4-addition mechanism can adopt a geometrically more favorable interaction[41] with the Criegee intermediate, allowing a near collinear geometry for the O–H···O moiety that increases the effectiveness of H-bonding and facilitates H-atom transfer and C–O bond formation. Equivalent transition states have been predicted for the reactions of Criegee intermediates with H_2SO_4 and the reactions are likely to be fast.[70] The larger rate constant for the CH_2OO reaction with water dimer over that of the monomer can also be justified by geometrical considerations and the relaxed seven-membered transition state.[31,32,34,35]

Tobias and Ziemann found that the relative rates for reactions of the C13 Criegee intermediate with hydroperoxide-forming species correlated well with the gas-phase acidities, ΔH_{acid}, but not with the OH bond strengths, ΔH_{bond}, indicating that the reactions proceeded via highly polar transition states.[69] Figure 5 show Hammett-like plots, equivalent to that of Tobias and Ziemann, showing the correlation of ΔH_{acid} and ΔH_{bond} with ln(k) for 1,2-addition reactions (H_2O, ROH, and HCl) and 1,4-addition reactions (HNO_3, RCOOH, $(H_2O)_2$) involving CH_2OO. The rate constants are taken from the recent

literature for reactions with water and water dimer,[13,14,17], carboxylic acids,[24,25] and inorganic acids[23] and are restricted to direct measurements. Values for ΔH_{acid} and ΔH_{bond} are taken from the ATcT database where available,[71] and also from collision-induced dissociation measurements by DeTuri and Ervin for the alcohols.[72] For water dimer, the gas phase acidity was approximated from estimates of the binding energy of the hydroxide-water complex $[(OH^-)H_2O]$.[73,74] The gas phase acidity values are summarized in Table 2, alongside the rate constants determined from direct kinetics measurements, and *ab initio* values of the transition state dipole moments.

As in the earlier work by Tobias and Ziemann,[69] we find a reasonably strong correlation between ΔH_{acid} and ln(k) as shown in Figure 5(a). Faster reactions are associated with reactants that have smaller values of gas-phase acidity and reactant ΔH_{acid} is a predictor of likely reactivity with CH_2OO. The rate constant for the $CH_2OO + H_2O$ reaction is a significant outlier, however. Furthermore, Hammett plots are strictly valid only for a single reaction mechanism. Figure 5(b) shows the relationship between ΔH_{bond} for OH (or HCl) and ln(k); as noted by Tobias and Ziemann, the correlation overall is poor, but the data naturally separate into the reactions that proceed via 1,2-addition and those that proceed via the 1,4-addition mechanism. Within the set of reactions that proceed via a specific mechanism, the rate constants generally increase as the bond strength decreases, but non-linearly. For the 1,2-addition reactions, the relationships of ln(k) with ΔH_{acid} and ΔH_{bond} shown in Figure 5(a) and (b) have opposite curvatures. We report, as an empirical observation, that ln(k) for the 1,2-addition reaction correlates strongly with the geometric mean of ΔH_{acid} and ΔH_{bond}, as shown in Figure 5(c). For the 1,4-addition reactions, which are generally characterized by larger rate constants for an equivalent bond strength or gas-phase acidity, the general trends are the same, but the curvature is universally negative, suggesting that the rate constants are converging on a limit. As noted earlier, the rate constants for the faster barrierless (or effectively barrierless) reactions may be controlled instead by long-range attractive interactions between the Criegee intermediate and the reactant molecules.

The *ab initio* calculations for the alcohol reactions show the formation of alkoxymethyl hydroperoxides, in agreement with the products seen in gas-phase ethene ozonolysis experiments using hydroxylic compounds as Criegee intermediate scavengers.[27,28] The calculations identify two pathways for the decomposition of the alkoxymethyl hydroperoxides products: a barrierless cleavage of the peroxide bond and a water elimination reaction. The former yields the radicals OH and $ROCH_2O$, and while energetically accessible, is unlikely to be significant at higher pressures which will allow collisional stabilization of the hydroperoxide. Any $ROCH_2O$ radicals produced, however, will react promptly with O_2 to yield HO_2 radicals and the corresponding alkyl formate.[75] The second pathway, in which water is eliminated to produce an alkyl formate, has a large free energy and enthalpic barrier ($\Delta H \approx \Delta G \approx +45$ kcal mol^{-1}) relative to alkoxymethyl hydroperoxide. While the enthalpy of the elimination transition state lies slightly below the reactant asymptote, a true barrier exists on the free energy surface that is +10 kcal mol^{-1} above the reactant asymptote. This decomposition pathway is also unlikely, particularly in collisional environments that favor stabilization of the alkoxymethyl hydroperoxide. Neeb *et al*. detected trace amounts of methyl formate (CH_3OCHO) from ethene ozonolysis in the presence of methanol,[28] but suggested that it resulted from heterogenous chemistry. However, methyl formate production is also possible from reaction of methoxymethoxy (CH_3OCH_2O) radical with O_2, which was also present in the reaction mixture.[75]

Finally, we consider the possible role of reactions between Criegee intermediates and alcohols in the atmosphere. While reaction with water vapor is the major global atmospheric sink for CH_2OO, recent studies have suggested that reactions with trace atmospheric gases may be locally competitive under certain conditions.[23] At 295 K and 50% relative humidity (RH), the loss rate of CH_2OO due to water vapor is about 2000 s^{-1}, with water dimer (~1900 s^{-1}) dominating over water monomer (~90 s^{-1}).[13,14,17] In sharp contrast, CH_2OO loss rates due to reactions with alcohols are estimated to be < 0.1 s^{-1} for typical alcohol concentrations consistent with urban environments (20 ppbv for methanol,

and 10 ppbv for ethanol and isopropanol) and consequently are uncompetitive even under exceptionally dry conditions. McGillen *et al*. found a negative temperature dependence for reaction of CH_2OO with methanol and ethanol, likely due to formation of moderately stable entrance channel complexes.[68] However, at lower temperatures the rate remains minor relative to reaction with water vapor, which continues to dominate. The measured rate constants for the CH_2OO + ROH reactions are an order of magnitude smaller than previous estimates for hydroxylic compounds used in box modelling,[76,77] although substitution of the Criegee intermediate can profoundly affect reactivity.[33]

Conclusions

Rate constants for the reactions of a series of alcohols with the Criegee intermediate CH_2OO have been measured at 295 K using transient absorption spectroscopy. Alcohols react more rapidly than water monomer, but much more slowly than carboxylic acids, with rate constants of order 10^{-13} cm^3 s^{-1}. For the reactions of water and alcohols, complementary *ab initio* calculations find entrance channel complexes and free energy barriers of ~10 kcal mol^{-1} that qualitatively explain the observed rate constants and reactivity trends among hydroxylic compounds. The transition state geometries and imaginary modes indicate that mechanism for the reactions of CH_2OO with alcohols and water can be viewed as a 1,2-addition, while carboxylic acids undergo 1,4-addition across the Criegee intermediate. Both mechanism lead to formation of substituted hydroperoxides. The rate constants for reactions of CH_2OO with hydroxylic compounds correlate reasonably well with the gas-phase acidities of the reactants, indicating highly polar transition states, as confirmed by the *ab initio* calculations. Under typical atmospheric conditions, alcohols are likely to make a negligible contribution to Criegee intermediate loss rates in the atmosphere.

Acknowledgements

We are grateful to AirUCI for support.

References

(1) Hatakeyama, S.; Akimoto, H. Reactions of Criegee Intermediates in the Gas Phase. *Res. Chem. Intermediat.* **1994**, *20* (3–5), 503–524.

(2) Johnson, D.; Marston, G. The Gas-Phase Ozonolysis of Unsaturated Volatile Organic Compounds in the Troposphere. *Chem. Soc. Rev.* **2008**, *37* (4), 699–716.

(3) Criegee, R. Mechanism of Ozonolysis. *Angew. Chem. Int. Ed.* **1975**, *14* (11), 745–752.

(4) Taatjes, C. A.; Meloni, G.; Selby, T. M.; Trevitt, A. J.; Osborn, D. L.; Percival, C. J.; Shallcross, D. E. Direct Observation of the Gas-Phase Criegee Intermediate (CH_2OO). *J. Am. Chem. Soc.* **2008**, *130* (36), 11883–11885.

(5) Welz, O.; Savee, J. D.; Osborn, D. L.; Vasu, S. S.; Percival, C. J.; Shallcross, D. E.; Taatjes, C. A. Direct Kinetic Measurements of Criegee Intermediate (CH_2OO) Formed by Reaction of CH_2I with O_2. *Science* **2012**, *335* (6065), 204–207.

(6) Eskola, A. J.; Wojcik-Pastuszka, D.; Ratajczak, E.; Timonen, R. S. Kinetics of the Reactions of CH_2Br and CH_2I Radicals with Molecular Oxygen at Atmospheric Temperatures. *Phys. Chem. Chem. Phys.* **2006**, *8* (12), 1416–1424.

(7) Taatjes, C. A.; Welz, O.; Eskola, A. J.; Savee, J. D.; Scheer, A. M.; Shallcross, D. E.; Rotavera, B.; Lee, E. P. F.; Dyke, J. M.; Mok, D. K. W.; et al. Direct Measurements of Conformer-Dependent Reactivity of the Criegee Intermediate CH_3CHOO. *Science* **2013**, *340* (6129), 177–180.

(8) Huang, H.-L.; Chao, W.; Lin, J. J.-M. Kinetics of a Criegee Intermediate That Would Survive High Humidity and May Oxidize Atmospheric SO_2. *Proc. Nat. Acad. Sci.* **2015**, *112* (35), 10857–10862.

(9) Liu, F.; Beames, J. M.; Green, A. M.; Lester, M. I. UV Spectroscopic Characterization of Dimethyl- and Ethyl-Substituted Carbonyl Oxides. *J. Phys. Chem. A* **2014**, *118* (12), 2298–2306.

(10) Taatjes, C. A.; Shallcross, D. E.; Percival, C. J. Research Frontiers in the Chemistry of Criegee Intermediates and Tropospheric Ozonolysis. *Phys. Chem. Chem. Phys.* **2014**, *16* (5), 1704–1718.

(11) Osborn, D. L.; Taatjes, C. A. The Physical Chemistry of Criegee Intermediates in the Gas Phase. *Int. Rev. Phys. Chem.* **2015**, *34* (3), 309–360.

(12) Taatjes, C. A. Criegee Intermediates: What Direct Production and Detection Can Teach Us About Reactions of Carbonyl Oxides. *Annu. Rev. Phys. Chem.* **2017**, *68* (1), 183–207.

(13) Berndt, T.; Kaethner, R.; Voigtländer, J.; Stratmann, F.; Pfeifle, M.; Reichle, P.; Sipilä, M.; Kulmala, M.; Olzmann, M. Kinetics of the Unimolecular Reaction of CH_2OO and the Bimolecular Reactions with the Water Monomer, Acetaldehyde and Acetone under Atmospheric Conditions. *Phys. Chem. Chem. Phys.* **2015**, *17* (30), 19862–19873.

(14) Chao, W.; Hsieh, J.-T.; Chang, C.-H.; Lin, J. J.-M. Direct Kinetic Measurement of the Reaction of the Simplest Criegee Intermediate with Water Vapor. *Science* **2015**, *347* (6223), 751–754.

(15) Stone, D.; Blitz, M.; Daubney, L.; Howes, N. U. M.; Seakins, P. Kinetics of CH_2OO Reactions with SO_2, NO_2, NO, H_2O and CH_3CHO as a Function of Pressure. *Phys. Chem. Chem. Phys.* **2013**, *16* (3), 1139–1149.

(16) Lewis, T. R.; Blitz, M. A.; Heard, D. E.; Seakins, P. W. Direct Evidence for a Substantive Reaction between the Criegee Intermediate, CH_2OO, and the Water Vapour Dimer. *Phys. Chem. Chem. Phys.* **2015**, *17* (7), 4859–4863.

(17) Smith, M. C.; Chang, C.-H.; Chao, W.; Lin, L.-C.; Takahashi, K.; Boering, K. A.; Lin, J. J.-M. Strong Negative Temperature Dependence of the Simplest Criegee Intermediate CH_2OO Reaction with Water Dimer. *J. Phys. Chem. Lett.* **2015**, *6* (14), 2708–2713.

(18) Sheps, L.; Scully, A. M.; Au, K. UV Absorption Probing of the Conformer-Dependent Reactivity of a Criegee Intermediate CH_3CHOO. *Phys. Chem. Chem. Phys.* **2014**, *16* (48), 26701–26706.

(19) Lin, L.-C.; Chao, W.; Chang, C.-H.; Takahashi, K.; Lin, J. J.-M. Temperature Dependence of the Reaction of *Anti*-CH_3CHOO with Water Vapor. *Phys. Chem. Chem. Phys.* **2016**, *18* (40), 28189–28197.

(20) Chhantyal-Pun, R.; Welz, O.; Savee, J. D.; Eskola, A. J.; Lee, E. P. F.; Blacker, L.; Hill, H. R.; Ashcroft, M.; Khan, M. A. H.; Lloyd-Jones, G. C.; et al. Direct Measurements of Unimolecular and Bimolecular Reaction Kinetics of the Criegee Intermediate $(CH_3)_2COO$. *J. Phys. Chem. A* **2017**, *121* (1), 4–15.

(21) Chhantyal-Pun, R.; Davey, A.; Shallcross, D. E.; Percival, C. J.; Orr-Ewing, A. J. A Kinetic Study of the CH_2OO Criegee Intermediate Self-Reaction, Reaction with SO_2 and Unimolecular Reaction Using Cavity Ring-down Spectroscopy. *Phys. Chem. Chem. Phys.* **2015**, *17* (5), 3617–3626.

(22) Fang, Y.; Liu, F.; Barber, V. P.; Klippenstein, S. J.; McCoy, A. B.; Lester, M. I. Communication: Real Time Observation of Unimolecular Decay of Criegee Intermediates to OH Radical Products. *J. Chem. Phys.* **2016**, *144* (6), 061102.

(23) Foreman, E. S.; Kapnas, K. M.; Murray, C. Reactions between Criegee Intermediates and the Inorganic Acids HCl and HNO_3 : Kinetics and Atmospheric Implications. *Angew. Chem. Int. Ed.* **2016**, *55* (35), 10419–10422.

(24) Welz, O.; Eskola, A. J.; Sheps, L.; Rotavera, B.; Savee, J. D.; Scheer, A. M.; Osborn, D. L.; Lowe, D.; Murray Booth, A.; Xiao, P.; et al. Rate Coefficients of C1 and C2 Criegee Intermediate Reactions with Formic and Acetic Acid Near the Collision Limit: Direct Kinetics Measurements and Atmospheric Implications. *Angew. Chem. Int. Ed.* **2014**, *126* (18), 4635–4638.

(25) Chhantyal-Pun, R.; McGillen, M. R.; Beames, J. M.; Khan, M. A. H.; Percival, C. J.; Shallcross, D. E.; Orr-Ewing, A. J. Temperature-Dependence of the Rates of Reaction of Trifluoroacetic Acid with Criegee Intermediates. *Angew. Chem. Int. Ed.* **2017**, *56* (31), 9044–9047.

(26) Su, F.; Calvert, J. G.; Shaw, J. H. A FT IR Spectroscopic Study of the Ozone-Ethene Reaction Mechanism in Oxygen-Rich Mixtures. *J. Phys. Chem.* **1980**, *84* (3), 239–246.

(27) Wolff, S.; Boddenberg, A.; Thamm, J.; Turner, W. V.; Gäb, S. Gas-Phase Ozonolysis of Ethene in the Presence of Carbonyl-Oxide Scavengers. *Atmos. Environ.* **1997**, *31* (18), 2965–2969.

(28) Neeb, P.; Horie, O.; Moortgat, G. K. Gas-Phase Ozonolysis of Ethene in the Presence of Hydroxylic Compounds. *Int. J. Chem. Kinet.* **1996**, *28* (10), 721–730.

(29) Vereecken, L.; Francisco, J. S. Theoretical Studies of Atmospheric Reaction Mechanisms in the Troposphere. *Chem. Soc. Rev.* **2012**, *41* (19), 6259–6293.

(30) Aplincourt, P.; Ruiz-López, M. F. Theoretical Study of Formic Acid Anhydride Formation from Carbonyl Oxide in the Atmosphere. *J. Phys. Chem. A* **2000**, *104* (2), 380–388.

(31) Ryzhkov, A. B.; Ariya, P. A. A Theoretical Study of the Reactions of Carbonyl Oxide with Water in Atmosphere: The Role of Water Dimer. *Chem. Phys. Lett.* **2003**, *367* (3), 423–429.

(32) Ryzhkov, A. B.; Ariya, P. A. A Theoretical Study of the Reactions of Parent and Substituted Criegee Intermediates with Water and the Water Dimer. *Phys. Chem. Chem. Phys.* **2004**, *6* (21), 5042.

(33) Anglada, J. M.; González, J.; Torrent-Sucarrat, M. Effects of the Substituents on the Reactivity of Carbonyl Oxides. A Theoretical Study on the Reaction of Substituted Carbonyl Oxides with Water. *Phys. Chem. Chem. Phys.* **2011**, *13* (28), 13034–13045.

(34) Anglada, J. M.; Solé, A. Impact of the Water Dimer on the Atmospheric Reactivity of Carbonyl Oxides. *Phys. Chem. Chem. Phys.* **2016**, *18* (26), 17698–17712.

(35) Lin, L.-C.; Chang, H.-T.; Chang, C.-H.; Chao, W.; Smith, M. C.; Chang, C.-H.; Lin, J. J.-M.; Takahashi, K. Competition between H_2O and $(H_2O)_2$ Reactions with CH_2OO/CH_3CHOO. *Phys. Chem. Chem. Phys.* **2016**, *18* (6), 4557–4568.

(36) Crehuet, R.; Anglada, J. M.; Bofill, J. M. Tropospheric Formation of Hydroxymethyl Hydroperoxide, Formic Acid, H_2O_2, and OH from Carbonyl Oxide in the Presence of Water Vapor: A Theoretical Study of the Reaction Mechanism. *Chem. Eur. J.* **2001**, *7* (10), 2227–2235.

(37) Kuwata, K. T.; Hermes, M. R.; Carlson, M. J.; Zogg, C. K. Computational Studies of the Isomerization and Hydration Reactions of Acetaldehyde Oxide and Methyl Vinyl Carbonyl Oxide. *J. Phys. Chem. A* **2010**, *114* (34), 9192–9204.
(38) Anglada, J. M.; Aplincourt, P.; Bofill, J. M.; Cremer, D. Atmospheric Formation of OH Radicals and H_2O_2 from Alkene Ozonolysis under Humid Conditions. *ChemPhysChem* **2002**, *3* (2), 215–221.
(39) Long, B.; Cheng, J.-R.; Tan, X.; Zhang, W. Theoretical Study on the Detailed Reaction Mechanisms of Carbonyl Oxide with Formic Acid. *Journal of Molecular Structure: THEOCHEM* **2009**, *916* (1–3), 159–167.
(40) Raghunath, P.; Lee, Y.-P.; Lin, M. C. Computational Chemical Kinetics for the Reaction of Criegee Intermediate CH_2OO with HNO_3 and Its Catalytic Conversion to OH and HCO. *J. Phys. Chem. A* **2017**.
(41) Vereecken, L. The Reaction of Criegee Intermediates with Acids and Enols. *Phys. Chem. Chem. Phys.* **2017**, *19* (42), 28630–28640.
(42) IUPAC. Compendium of Chemical Terminology, 2nd ed. (the "Gold Book"). Compiled by A. D. McNaught and A. Wilkinson. Blackwell Scientific Publications, Oxford (1997). XML on-line corrected version: http://goldbook.iupac.org (2006-) created by M. Nic, J. Jirat, B. Kosata; updates compiled by A. Jenkins. ISBN 0-9678550-9-8. https://doi.org/10.1351/goldbook..
(43) Jacob, D. J.; Field, B. D.; Li, Q.; Blake, D. R.; de Gouw, J.; Warneke, C.; Hansel, A.; Wisthaler, A.; Singh, H. B.; Guenther, A. Global Budget of Methanol: Constraints from Atmospheric Observations. *J. Geophys. Res.* **2005**, *110* (D8), D08303.
(44) Heikes, B. G.; Chang, W.; Pilson, M. E. Q.; Swift, E.; Singh, H. B.; Guenther, A.; Jacob, D. J.; Field, B. D.; Fall, R.; Riemer, D.; et al. Atmospheric Methanol Budget and Ocean Implication. *Global Biogeochem. Cycles* **2002**, *16* (4), 1133.
(45) Kirstine, W. V.; Galbally, I. E. Ethanol in the Environment: A Critical Review of Its Roles as a Natural Product, a Biofuel, and a Potential Environmental Pollutant. *Crit. Rev. Env. Sci. Tech.* **2012**, *42* (16), 1735–1779.
(46) Colón, M.; Pleil, J. D.; Hartlage, T. A.; Lucia Guardani, M.; Helena Martins, M. Survey of Volatile Organic Compounds Associated with Automotive Emissions in the Urban Airshed of São Paulo, Brazil. *Atmos. Environ.* **2001**, *35* (23), 4017–4031.
(47) Nguyen, H. T.-H.; Takenaka, N.; Bandow, H.; Maeda, Y.; de Oliva, S. T.; Botelho, M. M. f.; Tavares, T. M. Atmospheric Alcohols and Aldehydes Concentrations Measured in Osaka, Japan and in Sao Paulo, Brazil. *Atmos. Environ.* **2001**, *35* (18), 3075–3083.
(48) König, G.; Brunda, M.; Puxbaum, H.; Hewitt, C. N.; Duckham, S. C.; Rudolph, J. Relative Contribution of Oxygenated Hydrocarbons to the Total Biogenic VOC Emissions of Selected Mid-European Agricultural and Natural Plant Species. *Atmos. Environ.* **1995**, *29* (8), 861–874.
(49) Foreman, E. S.; Kapnas, K. M.; Jou, Y.; Kalinowski, J.; Feng, D.; Gerber, R. B.; Murray, C. High Resolution Absolute Absorption Cross Sections of the $\tilde{B}^1A'$–$\tilde{X}^1A'$ Transition of the CH_2OO Biradical. *Phys. Chem. Chem. Phys.* **2015**, *17* (48), 32539–32546.
(50) Huang, H.; Eskola, A. J.; Taatjes, C. A. Pressure-Dependent I-Atom Yield in the Reaction of CH_2I with O_2 Shows a Remarkable Apparent Third-Body Efficiency for O_2. *J. Phys. Chem. Lett.* **2012**, *3* (22), 3399–3403.
(51) Huang, H.; Rotavera, B.; Eskola, A. J.; Taatjes, C. A. Correction to "Pressure-Dependent I Atom Yield in the Reaction of CH_2 I with O_2 Shows a Remarkable Apparent Third-Body Efficiency for O_2." *J. Phys. Chem. Lett.* **2013**, *4* (22), 3824–3824.
(52) Ting, W.-L.; Chang, C.-H.; Lee, Y.-F.; Matsui, H.; Lee, Y.-P.; Lin, J. J.-M. Detailed Mechanism of the $CH_2I + O_2$ Reaction: Yield and Self-Reaction of the Simplest Criegee Intermediate CH_2OO. *J. Chem. Phys.* **2014**, *141* (10), 104308.

(53) Huang, Y.-H.; Chen, L.-W.; Lee, Y.-P. Simultaneous Infrared Detection of the ICH_2OO Radical and Criegee Intermediate CH_2OO: The Pressure Dependence of the Yield of CH_2OO in the Reaction $CH_2I + O_2$. *J. Phys. Chem. Lett.* **2015**, *6* (22), 4610–4615.
(54) MOLPRO, Version 2012.1, a Package of Ab Initio Programs, H.-J. Werner, P. J. Knowles, G. Knizia, F. R. Manby, M. Schütz, P. Celani, T. Korona, R. Lindh, A. Mitrushenkov, G. Rauhut, K. R. Shamasundar, T. B. Adler, R. D. Amos, A. Bernhardsson, A. Berning, D. L. Cooper, M. J. O. Deegan, A. J. Dobbyn, F. Eckert, E. Goll, C. Hampel, A. Hesselmann, G. Hetzer, T. Hrenar, G. Jansen, C. Köppl, Y. Liu, A. W. Lloyd, R. A. Mata, A. J. May, S. J. McNicholas, W. Meyer, M. E. Mura, A. Nicklass, D. P. O'Neill, P. Palmieri, D. Peng, K. Pflüger, R. Pitzer, M. Reiher, T. Shiozaki, H. Stoll, A. J. Stone, R. Tarroni, T. Thorsteinsson, and M. Wang, , See http://www.molpro.net.
(55) Masaki, A.; Tsunashima, S.; Washida, N. Rate Constants for Reactions of Substituted Methyl Radicals (CH_2OCH_3, CH_2NH_2, CH_2I, and CH_2CN) with O_2. *J. Phys. Chem.* **1995**, *99* (35), 13126–13131.
(56) Sheps, L. Absolute Ultraviolet Absorption Spectrum of a Criegee Intermediate CH_2OO. *J. Phys. Chem. Lett.* **2013**, *4* (24), 4201–4205.
(57) Ting, W.-L.; Chen, Y.-H.; Chao, W.; Smith, M. C.; Lin, J. J.-M. The UV Absorption Spectrum of the Simplest Criegee Intermediate CH_2OO. *Phys. Chem. Chem. Phys.* **2014**, *16* (22), 10438–10443.
(58) Spietz, P.; Gómez Martín, J. C.; Burrows, J. P. Spectroscopic Studies of the I_2/O_3 Photochemistry: Part 2. Improved Spectra of Iodine Oxides and Analysis of the IO Absorption Spectrum. *J. Photochem. Photobio. A* **2005**, *176* (1–3), 50–67.
(59) Enami, S.; Sakamoto, Y.; Yamanaka, T.; Hashimoto, S.; Kawasaki, M.; Tonokura, K.; Tachikawa, H. Reaction Mechanisms of IO Radical Formation from the Reaction of CH_3I with Cl Atom in the Presence of O_2. *B. Chem. Soc. Jpn.* **2008**, *81* (10), 1250–1257.
(60) Gravestock, T. J.; Blitz, M. A.; Bloss, W. J.; Heard, D. E. A Multidimensional Study of the Reaction CH_2I+O_2: Products and Atmospheric Implications. *ChemPhysChem* **2010**, *11* (18), 3928–3941.
(61) Foreman, E. S.; Murray, C. Kinetics of IO Production in the $CH_2I + O_2$ Reaction Studied by Cavity Ring-Down Spectroscopy. *J. Phys. Chem. A* **2015**, *119* (34), 8981–8990.
(62) Roehl, C. M.; Burkholder, J. B.; Moortgat, G. K.; Ravishankara, A. R.; Crutzen, P. J. Temperature Dependence of UV Absorption Cross Sections and Atmospheric Implications of Several Alkyl Iodides. *J. Geophys. Res.* **1997**, *102* (D11), 12819–12829.
(63) Mössinger, J. C.; Shallcross, D. E.; Cox, R. A. UV-VIS Absorption Cross-Sections and Atmospheric Lifetimes of CH_2Br_2, CH_2I_2 and CH_2BrI. *J. Chem. Soc., Faraday Trans.* **1998**, *94* (10), 1391–1396.
(64) Olzmann, M.; Kraka, E.; Cremer, D.; Gutbrod, R.; Andersson, S. Energetics, Kinetics, and Product Distributions of the Reactions of Ozone with Ethene and 2,3-Dimethyl-2-Butene. *J. Phys. Chem. A* **1997**, *101* (49), 9421–9429.
(65) Newland, M. J.; Rickard, A. R.; Alam, M. S.; Vereecken, L.; Muñoz, A.; Ródenas, M.; Bloss, W. J. Kinetics of Stabilised Criegee Intermediates Derived from Alkene Ozonolysis: Reactions with SO_2, H_2O and Decomposition under Boundary Layer Conditions. *Phys. Chem. Chem. Phys.* **2015**, *17* (6), 4076–4088.
(66) Buras, Z. J.; Elsamra, R. M. I.; Green, W. H. Direct Determination of the Simplest Criegee Intermediate (CH_2OO) Self Reaction Rate. *J. Phys. Chem. Lett.* **2014**, *5* (13), 2224–2228.
(67) Su, Y.-T.; Lin, H.-Y.; Putikam, R.; Matsui, H.; Lin, M. C.; Lee, Y.-P. Extremely Rapid Self-Reaction of the Simplest Criegee Intermediate CH_2OO and Its Implications in Atmospheric Chemistry. *Nat. Chem.* **2014**, *6* (6), 477–483.
(68) McGillen, M. R.; Curchod, B. F. E.; Chhantyal-Pun, R.; Beames, J. M.; Watson, N.; Khan, M. A. H.; McMahon, L.; Shallcross, D. E.; Orr-Ewing, A. J. Criegee Intermediate–Alcohol Reactions, A Potential Source of Functionalized Hydroperoxides in the Atmosphere. *ACS Earth Space Chem.* **2017**.

(69) Tobias, H. J.; Ziemann, P. J. Kinetics of the Gas-Phase Reactions of Alcohols, Aldehydes, Carboxylic Acids, and Water with the C13 Stabilized Criegee Intermediate Formed from Ozonolysis of 1-Tetradecene. *J. Phys. Chem. A* **2001**, *105* (25), 6129–6135.
(70) Kurtén, T.; Bonn, B.; Vehkamäki, H.; Kulmala, M. Computational Study of the Reaction between Biogenic Stabilized Criegee Intermediates and Sulfuric Acid. *J. Phys. Chem. A* **2007**, *111* (17), 3394–3401.
(71) Ruscic, B. Active Thermochemical Tables (ATcT) Values Based on Ver. 1.122 of the Thermochemical Network; Available at ATcT.Anl.Gov. **2015**.
(72) DeTuri, V. F.; Ervin, K. M. Competitive Threshold Collision-Induced Dissociation: Gas-Phase Acidities and Bond Dissociation Energies for a Series of Alcohols. *J. Phys. Chem. A* **1999**, *103* (35), 6911–6920.
(73) Paul, G. J. C.; Kebarle, P. Thermodynamics of the Association Reactions $OH^- + H_2O \rightarrow HOHOH^-$ and $CH_3O^- + CH_3OH \rightarrow CH_3OHOCH_3^-$ in the Gas Phase. *J. Phys. Chem.* **1990**, *94* (12), 5184–5189.
(74) Price, E. A.; Robertson, W. H.; Diken, E. G.; Weddle, G. H.; Johnson, M. A. Argon Predissociation Infrared Spectroscopy of the Hydroxide–water Complex ($OH^-{\cdot}H_2O$). *Chem. Phys. Lett.* **2002**, *366* (3–4), 412–416.
(75) Orlando, J. J.; Tyndall, G. S.; Wallington, T. J. The Atmospheric Chemistry of Alkoxy Radicals. *Chem. Rev.* **2003**, *103* (12), 4657–4690.
(76) Vereecken, L.; Harder, H.; Novelli, A. The Reaction of Criegee Intermediates with NO, RO_2, and SO_2, and Their Fate in the Atmosphere. *Phys. Chem. Chem. Phys.* **2012**, *14* (42), 14682.
(77) Vereecken, L.; Harder, H.; Novelli, A. The Reactions of Criegee Intermediates with Alkenes, Ozone, and Carbonyl Oxides. *Phys. Chem. Chem. Phys.* **2014**, *16* (9), 4039–4049.

Tables

Table 1 *Ab initio* thermochemical data calculated at the CCSD(T)/aug-cc-pVDZ//CCSD/cc-pVDZ level of theory. All values are reported relative to the reactants. Values of E + ZPE are at 0 K, while values of ΔH and ΔG are at 298.15 K.

Alcohol	CH_3OH	C_2H_5OH	$(CH_3)_2CHOH$
		E + ZPE (ΔH) [ΔG] / kcal mol^{-1}	
Entrance channel complex	–7.4 (–7.5) [+2.0]	–7.9 (–8.4) [+2.9]	–8.0 (–8.5) [+2.9]
OH insertion, TS_{add}	–2.9 (–4.1) [+8.3]	–3.6 (–4.6) [+7.9]	–4.0 (–4.9) [+7.7]
Alkoxymethyl hydroperoxide (MMHP, EMHP, PMHP)	–45.6 (–46.4) [–34.8]	–48.2 (–48.9) [–37.1]	–47.5 (–48.1) [–36.1]
H_2O elimination, TS_{elim}	–0.8 (+10.5) {-0.1}	–0.7 (–1.2) [+10.1]	+0.2 (–0.8) [+12.3]
Alkyl formates + H_2O (MF, EF, PF)	–120.5 (–120.1) [–118.9]	–120.8 (–120.1) [–119.0]	–118.1 (–117.5) [–115.9]
Radicals + OH	–4.7 (–4.3) [–3.4]	–5.3 (–4.6) [–4.2]	–4.1 (–3.4) [–2.7]
CH addition $TS_{add,CH}$	+22.0 (+20.8) [+33.3]		
Alkoxymethyl hydroperoxide (2HEHP)	–49.9 (–51.0) [–38.6]		

Table 2 Rate constants, gas-phase acidities, and calculated transition state dipole moments (CCSD/cc-pVDZ) for reactions of CH_2OO with hydroxylic compounds and HCl. Values of ΔH_{acid} are taken from the Active Thermochemical Tables,[71] and have uncertainties of ≤ 0.1 kcal mol^{-1}, unless indicated. For the alcohols, the bottom ΔH_{acid} value is taken from DeTuri and Ervin[72] while the value for $(H_2O)_2$ is calculated from values reported by Paul and Kebarle[73] and Price et al.[74]

	k / 10^{-13} cm^3 s^{-1}	ΔH_{acid} / kcal mol^{-1}	μ_{TS} / D	References
CH_3OH	1.43±0.10	382.5 382±1	3.88	This work
C_2H_5OH	2.34±0.22	379.0 379±1	3.73	
$(CH_3)_2CHOH$	1.93±0.24	377±1	3.79	
H_2O	< 0.04 0.0032±0.0012 <0.015	390.3	3.95	Welz *et al.*[5] Berndt *et al.*[13] Chao *et al.*[14]
$(H_2O)_2$	65±8 40±12 74±6	367	4.74	Chao *et al.*[14] Lewis *et al.*[16] Smith *et al.*[17]
HCOOH	1100±100	344.8	3.45	Welz *et al.*[24]
CH_3COOH	1300±100 1200±100	348±1	3.59	
CF_3COOH	3400±300	324±3		Chhantyal-Pun *et al.*[25]
$HONO_2$	5400±1000	324.5	5.24	Foreman *et al.*[23]
HCl	460±100	333.4		

Figures

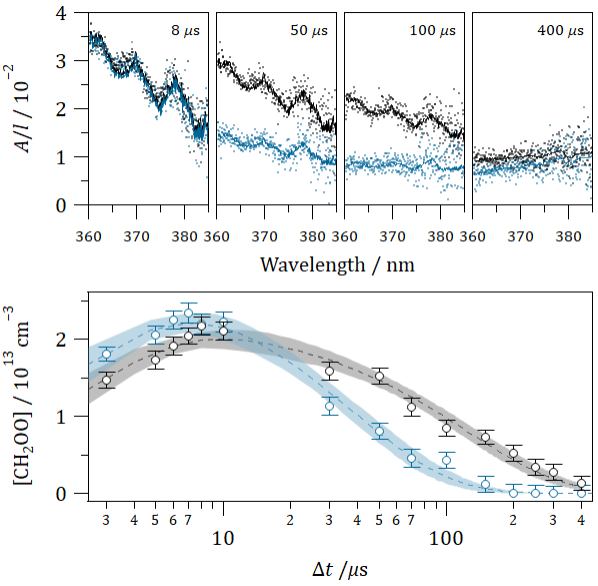

Figure 1. Top panel: transient absorption spectra recorded at the indicated time delays in the absence (black) and presence of 9.7×10^{16} cm^{-3} methanol (blue). Experimental data are represented as dots, with the best fit spectra (see text) shown as solid lines. The absorbance is dominated by CH_2OO at short delays and by IO at longer delays. The more rapid removal of the Criegee intermediate in the presence of methanol is apparent at intermediate delays as the loss of the characteristic vibrational structure. Bottom panel: [CH_2OO] time profiles determined from the transient absorption spectra and fits (dashed lines, with shaded areas representing 95% confidence intervals) to an exponential rise and fall.

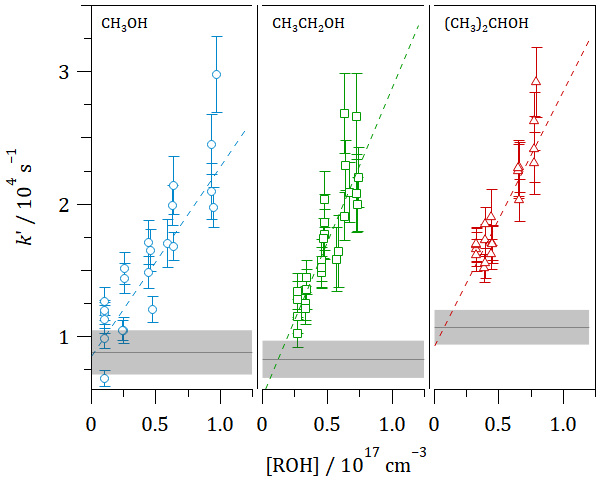

Figure 2. Pseudo-first order plots for reaction of CH_2OO with CH_3OH (blue), CH_3CH_2OH (green), and $(CH_3)_2CHOH$ (red) as indicated. The individual data points are shown with 1σ error bars representing the uncertainty in the fit of the corresponding $[CH_2OO]$ time profile. Linear fits to each data set are shown as dashed lines. The solid horizontal black line denotes k_0', the background loss rate in the absence of alcohol, with shading used to represent the uncertainty.

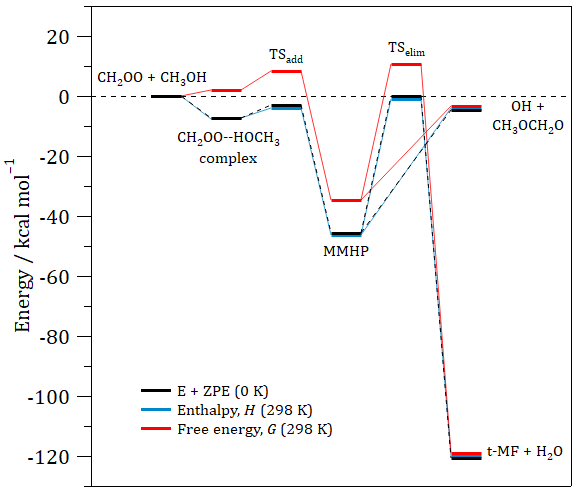

733

734 Figure 3. *Ab initio* calculated energy (E + ZPE) at 0 K (black), enthalpy (blue), and free
735 energy (red) at 298.15 K profiles for the $CH_2OO + CH_3OH$ reaction. TS_{add} and TS_{elim} are
736 the transition states for the initial addition reaction to form methoxymethyl
737 hydroperoxide (MMHP) and the subsequent water elimination reaction that may lead
738 to production of methyl formate (MF).

739

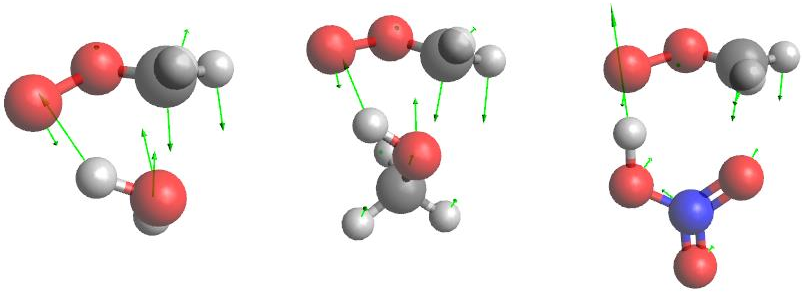

Figure 4 Transition state structures and force vectors for the reactions of CH_2OO with H_2O, CH_3OH, and HNO_3 calculated at the CCSD/cc-pVDZ level of theory.

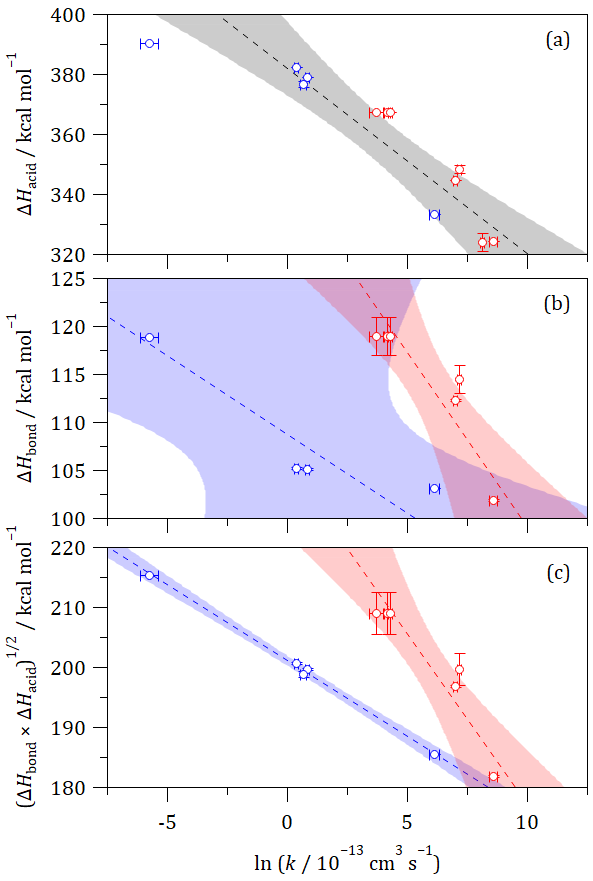

743

744 Figure 5 Hammett-like plots showing correlations between reactant (a) bond energy,
745 ΔH_{bond}, (b) gas-phase acidity, ΔH_{acid}, and (c) the geometric mean ΔH_{bond} and ΔH_{acid}, and
746 ln(k) for CH_2OO addition reactions. Points shown in red correspond to reactions that
747 proceed via 1,4-addition (water, carboxylic acids, nitric acid), while points shown in
748 blue correspond to reactions that proceed via 1,2-addition (water monomer, alcohols,
749 hydrochloric acid), as described in the text.

750